Chemical Engineering Journal 528 (2026) 172387

Contents lists available at ScienceDirect

Chemical Engineering Journal

journal homepage: www.elsevier.com/locate/cej

Renewable energy powered membrane technology: Design of a photovoltaic hybrid ultra- and nanofiltration membrane mobile laboratory

Bryce S. Richards [a], Youssef-Amine Boussouga [b,1], Emmanuel.O. Ogunniyi [a], Andrea I. Schäfer [b,*]

[a] Institute of Microstructure Technology (IMT), Karlsruhe Institute of Technology (KIT), Hermann von Helmholtz Platz 1, 76344, Eggenstein-Leopoldshafen, Germany
[b] Institute for Advanced Membrane Technology (IAMT), Karlsruhe Institute of Technology (KIT), Hermann von Helmholtz Platz 1, 76344, Eggenstein-Leopoldshafen, Germany

ARTICLE INFO

Keywords:
Mobile laboratory
Photovoltaic-powered membrane filtration system
Desalination
Safe operating window (SOW)
Supercapacitor energy storage
Uranium removal
Concentration polarization

ABSTRACT

The design, construction, and performance testing of a mobile, photovoltaic-powered, hybrid filtration system, equipped with both micro-filters and nanofiltration (NF) membranes is described. This 'mobile lab' enables autonomous research with a wide range of water sources – from desalination of brackish water to treatment of contaminated low salinity groundwater. Firstly, the system performance was investigated as a function of five different NF membranes and feedwater salinity (1–20 g/L). The importance of choosing the correct set-point in operating pressure for experiments is discussed in order to map out the safe operating window (SOW) of different system configurations (membranes, feed waters). Secondly, a case study was conducted using real water contaminated with naturally-occurring uranium, where the system was able to treat the water to achieve the World Health Organization guideline values at a specific energy consumption of 1 kWh/m^3. The benefit of using supercapacitor energy storage for buffering solar power fluctuations was explored. Despite testing a wide salinity range, the system was observed to achieve drinking water standards at salinities as low as 5 g/L with the NF90 membrane, clearly defining a SOW for treating primarily brackish water. Three membranes exhibited limited salt retention and only achieved satisfactory performance at the lowest NaCl salinity (1 g/L), Overall, this work helps pave the way for the design of photovoltaic-powered membrane filtration systems for both mobile (disaster relief) and stationary (drinking water provision in remote areas) scenarios supported by research that enables field work and excellent research training opportunities to contribute to solving global challenges.

1. Introduction

According to the latest United Nations Sustainable Development Goals report, about 2.1 billion people still lacked access to a safely managed drinking water source in 2024 [1], noting that this does not imply that the water is treated. At the same time, the number of people without access to electricity in the world decreased only slightly to 666 million [2]. While the exact overlap between these two groups remains unknown, strong correlations linking the two have been observed in the past [3]. For this reason, water treatment technologies that can be powered directly from renenwable energy resources seem to be the best way to break out of this paradigm [4]. Indeed, the market for solar-powered desalination systems is expected to reach US$4.8 billion by the year 2031, exhibiting an annual growth rate of 7.7 % [5]. In particular, photovoltaic-powered membrane filtration (PV-membrane) systems are a promising option for the decentralised provision of drinking water in remote areas, which lack connection to either a reliable electricity grid or water distribution network. Such PV-membranes systems are becoming increasingly popular due to modularity, energy efficiency and robustness, with small-scale units (producing <3 m^3 per day) filtering brackish water with a salinity of 5 g/L total dissolved solids (TDS) at a specific energy consumption (SEC) of about 3–4 kWh/m^3 [6] and with a targeted system lifetime of 20 years [7]. The PV modules produce clean electricity from sunlight to power the pump in the system, while a range of pressure-driven membranes can be employed to remove the desired contaminants from the available water source. For example, ultrafiltration (UF) membranes typically remove particles, viruses and bacteria, while nanofiltration (NF) or reverse

* Corresponding author.
E-mail address: andrea.iris.schaefer@kit.edu (A.I. Schäfer).
[1] Current affiliation (Y.-A. Boussouga): International Water Research Institute (IWRI), Mohammed VI Polytechnic University (UM6P), Benguerir, Morocco, youssef-amine.boussouga@um6p.ma

https://doi.org/10.1016/j.cej.2025.172387
Received 15 October 2025; Received in revised form 22 December 2025; Accepted 27 December 2025
Available online 30 December 2025

osmosis (RO) membranes are for desalination, primarily retaining multivalent and monovalent ions, respectively. The compact nature of the technology also lends itself for disaster-relief applications, for example, with 14 PV-powered UF systems (US$25000) being deployed in Haiti after the 2010 earthquake [8,9].

Such work presents an excellent opportunity for out-of-the-laboratory student engagement and training, with design aspects and fieldwork challenges offering much needed graduate skills. Schäfer and Richards have been involved in the research on the development of PV-membrane systems for nearly 25 years, briefly summarised as follows [10]:

- Prototype I (2001) – the authors' first proof-of-concept PV-membrane system [11] built by a team of interdisciplinary Bachelor students [10];
- Prototype II (2002) – based on a submerged UF module and a 2.5″ low-pressure RO membrane and powered by 255 W of PV modules during testing in the Australian outback [12];
- Prototype III (2004) – involved upscaling to large area UF and 4" NF/RO membranes as well as a higher-pressure direct-current (DC) pump, but was not powered by PV [13];
- Prototype IV (2004) – was based on the previous version, but added air bubbling for UF membrane cleaning and a data logging system and was tested for trace contaminant removal in an Australian national park [14];
- Prototype V (2005) – an autonomous system redesigned around a custom-made submersible 3-phase DC borehole pump together with an industry partner. Prototype V is mounted onto an off-road trailer and equipped with 300 W of PV panels as well as a solar-tracker [15] and controlled via LabView software. This system was extensively field-tested for treating brackish water in outback Australia [16], as a wind-powered version for desalination in Scotland [17], and for fluoride removal in northern Tanzania [18]; and
- Prototype VI (2017) – a redesigned system with improvements being made on the hydraulic side – e.g. a 4″ pressure-driven UF module with backwash – as well as enhanced electrics, e.g. through solar-array simulator and sensors, as well as energy storage options (lithium ion batteries or supercapacitors) and an industrial control system [19].

This work describes prototype VII, a mobile version of prototype VI that is designed to be a towed by a Land Rover Defender 130 four-wheel drive vehicle to enable field-testing at remote sites – as illustrated in Fig. 1. Previous system prototypes were focused only on brackish water desalination; however, the present system is designed to be more flexible, now also allowing for surface water treatment. While the technology per se might not seem new, the novelty here is to; i) realise an autonomous mobile laboratory that can be employed for field work, enabling treating challenging water sources in remote relocations; where: ii) the water treatment technologies can be exchanged (e.g. NF membranes in this work, with single-pass electrodialysis being a current alternative [20]); and iii) different energy storage options can be trialled (compared to the directly-coupled configuration); while iv) still allowing for the solar irradiance to be controlled, thus facilitating comparison between different membranes. Specifically, prototype VII benefits from experienced gained via the development of prototypes I – VI, specifically: i) being able to readily interchange membranes to enable treatment of a wide range of water sources; ii) enabling daily permeate production typically in the range of 1–3 m^3 per solar day; iii) having PV panels integrated into the roof of the trailer in a TÜV-certified design for ease of transport and rapid deployment; iv) significant energy storage capacity (2.5 kWh of supercapacitors and 2.4 kWh of lithium ion batteries); as well as v) integrated datalogging and system control via an industrial programmable logic controller. The design of the system along with the choice of components is discussed in detail below – along with testing of the system's capabilities.

In particular, uranium (U) removal from natural water by NF, which has been investigated from laboratory to pilot scale, is strongly affected by water chemistry – especially pH due to U speciation [21], and the nature of coexisting ligands [22] – as well as the membrane material [23]. Rossiter et al. demonstrated this complexity in a PV-membrane system operated to treat a feed water containing 780 μg/L of U yielded a permeate of about 67 μg U/L – above the WHO limit – due to U accumulation and eventual permeation through the membrane [24]. The adsorption of U in NF membranes – primarily resulting from the attachment of positively charged U(VI) complexes, such as $(UO_2)_3(OH)_5^+$ and $(UO_2)_4(OH)_7^+$ formed at pH 5–7, to negatively charged functional groups (e.g. COO^- in polyamide NF membranes [25]), should be carefully considered when operating NF in PV-membrane systems, especially to enhance process reliability during fluctuating PV power supply conditions.

To evaluate PV-membrane system performance, experiments are conducted using five different NF membranes and two different waters: i) synthetic water ranging with salinities ranging from 0.5 g/L TDS to very brackish (20 g/L TDS); as well as ii) a naturally occurring U containing water. By conducting experiments on the PV-membrane system performance as a function of the set-point operating pressure, the safe operating window (SOW) could be mapped out under all operating conditions. The SOW enables a better understanding of how each membrane performs under a wide range of hydraulic conditions – specifically flux and transmembrane pressure (TMP) – which enables the optimum NF membrane to be chosen for each water type. Finally, as an example, the system performance with regard to U removal – sourced from natural spring water that contains an elevated uranium concentration of ~50 μg/L – over a typical solar day was investigated along with the potential for enhanced performance when using supercapacitor

Fig. 1. Mobile lab equipped with the PV-membrane system (prototype VII) that is towed by a Land Rover Defender 130 for fieldwork in remote areas.

energy storage. The evaluation is an example for the utilization of the mobile laboratory with a broad range of waters. It should be noted that the mobile lab was deliberately designed *not* to be able to treat seawater given that: i) small-scale PV-powered seawater reverse osmomis systems have been widely deployed in marine vessels; ii) such systems do not need to exhibit flexible design given that the composition of seawater is very similar world-wide [26]; and iii) there are many inland regions of continents – far from the coast – where non-potable water supplies (whether brackish groundwater or contaminated surface water) are abundant and there is an excellent synergy with the amount of available sunshine [3,11]. The research objectives of this work are defined as follows:

- To design of Prototype VII and conduct full testing using five different types of NF membranes for brackish water desalination (feedwater salinities ranging from 1 to 20 g/L);
- To map out the SOW of Prototype VII in different configurations (membranes, feedwater salinity) under steady-state conditions;
- To determine the removal efficiency of a specific contaminant (naturally-occurring uranium) and compare it to World Health Organization (WHO) guidelines; and to
- To evaluate the added benefit of supercapacitor energy buffering in stabilising PV-membrane system performance during rapid fluctuations in solar irradiance.

2. PV-membrane system design as a mobile lab

2.1. Mobile lab design criteria

Given that the quality of many water sources to be treated in future field research may range from surface waters to brackish groundwaters with a suite of contaminants, prototype VII of the PV-membrane system was designed to be as flexible and powerful as possible. In terms of water treatment, this meant producing 1–3 m^3 of permeate from a wide range of feedwaters and operating pressures of up to 20 bar. In addition, the system that is mounted onto the trailer should: i) be modular, enabling other water treatment technologies also to be developed and tested in the future; and ii) fit onto a standard wooden transport pallet (120 cm long × 80 cm wide) for ease of transport.

2.2. Trailer design

As illustrated in Fig. S1 in the Supplementary Information, the twin-axle design has a floor area of 300 cm (length) × 135 cm (width) × 140 cm (height) and a maximum laden weight of 3500 kg, while the empty trailer itself weighs 920 kg. It is equipped with off-road tyres and shock absorbers facilitate transportation over rough terrain. The rear door of the trailer opens fully for loading/unloading of equipment (ramps are mounted to the front of the trailer along with a toolbox), while the two side doors swing up for ease of access when conducting experiments in the field. All doors lock for security, while steel legs at each corner provide extra stability under windy conditions.

2.3. PV-membrane system design

The PV-membrane system is designed to treat a wide range of feedwater sources, ranging from contaminated surface water to brackish groundwater with salinities up to 20 g/L TDS (osmotic pressure of 16.9 bar at 25 °C). This upper treatment limit is dictated by the maximum operating pressure of the system (20 bar). The treatment of seawater is therefore deliberately excluded. A system schematic is provided in Fig. 2. The system has a customised high-density polyethylene (HDPE) feed tank (RDM Producten, Netherlands), in which a helical rotary pump (Grundfos SQFlex 0.6-3 N, Denmark) is submerged. The selected pump has a maximum power consumption of $P = 580$ W, operates on 30–300 V_{DC}, and can generate a maximum pressure of 20 bar. Hence, 20 bar is the maximum operating pressure of the system. The "N" model of the pump was chosen for extra corrosion resistance. For back-pressure control, an actuator-controlled needle valve (MCM-S50AF-3-SS-18RF8, Hanbay Inc., USA) is installed in the concentrate stream. For safe operation (protection from overpressure), a pressure relief valve set to 25 bar (460tGFL-15-m/f-15/15 – EPDM, Goetze KG Armaturen, Germany) is installed. For completeness, two additional system schematics are provided in the Supplementary Information (Figs. S2 and S3), while full lists the of hydraulic and electrical system components are provided in Tables S1 and S2, respectively.

As shown in Fig. 2, system control and data collection are realised via a programmable logic controller (PLC, Unistream 10.4″, Unitronics, Israel). The PLC is programmed to control the switching operation of the PV, SCs and the pump via the integrated solid-state relays. The PLC can log the analogue input data (4–20 mA) from up to 40 sensors. The outputs of the sensors are fed into the data acquisition (DAQ) unit of the PLC for further processing, logging and control operations. The signals from the following sensors are fed into the PLC. For water quality monitoring the following sensors were used; high-pressure electrical conductivity (EC) sensors for feed and concentrate (Type 4221, Valmet,

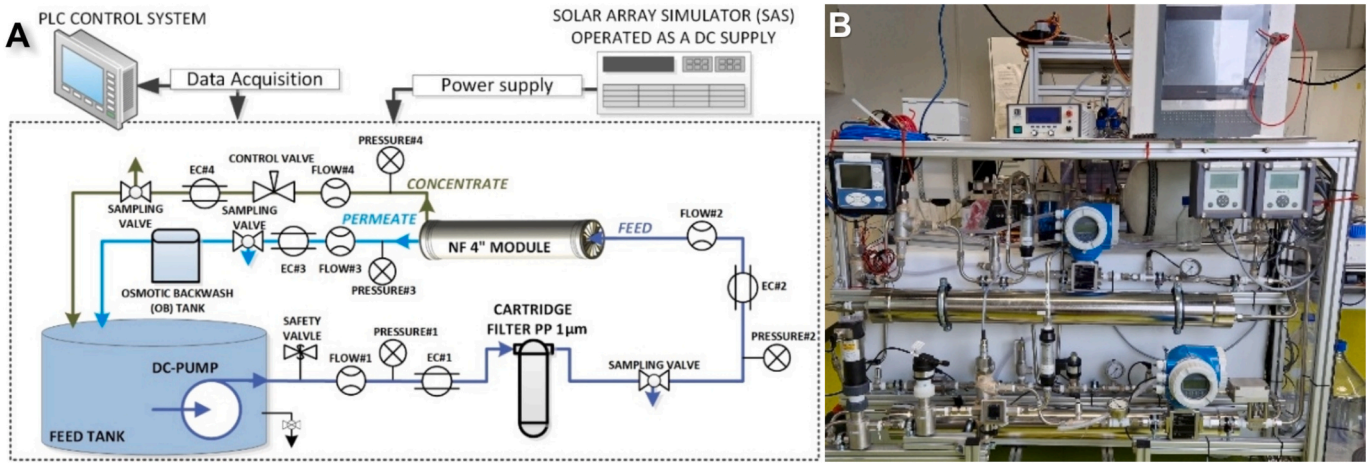

Fig. 2. (A) Schematic of the mobile PV-membrane system (prototype VII). The DC high-pressure pump is submerged in the feed tank, wherefrom feedwater is driven first through the micro-filter (or UF module) before passing through the NF membrane module for desalination. Power can be supplied via the PV panels, or a solar array simulator (SAS) can be used to emulate PV power. Three sensors – flow, pressure electrical conductivity (EC), plus potentially pH (not shown here) – are installed on the feed, permeate and concentrate streams. (B) Photograph of the PV-membrane system before it is loaded into the trailer.

Finland); EC sensor (Type 8222, Bürket, Germany) for NF permeate; high-pressure pH sensor (3300HTVP-10-30, Emerson, USA) for feed; pH sensor (Type 8202, Bürket, Germany) for NF permeate; and turbidity sensor (Type STS 1–20 mm, Seli, Germany) for NF feed. For calibration of EC and pH sensors, an EC standard (KCl 12.8 mS/cm at 25 °C, Certipur®, Merck, Germany) and buffer solutions (pH 4.01, 7.00, and 11.00 at 25 °C, Certipur®, Merck, Germany) were used, respectively. For monitoring system operation: high-pressure flow sensors (Promag H300 5H3B08-MJL4/0, Endress Hauser, Switzerland) for feed and concentrate, bi-directional flow sensor (MIM-1203HG4C3TO, Kobold, Germany) for permeate, pressure sensors (Type 8316, Bürket, Germany), flow meter (SFF-L00005-B08, Bibus, Germany), pressure gauge (MAN-RD27B9, Kobold, Germany). A sample valve (H-99S-00-SS-L-R-1/2 LF, Ham-Let, Germany) is used for accessing the feedwater after the pre-filter/UF membrane. The operation of the system is detailed step-by-step in Tables S1 - S3.

2.4. Pre-treatment options and membrane selection

Standard 4″ diameter (4040) membranes are employed in two stages – a pressure-driven UF membrane (DuPont dizzer/TapTec P4040–6.0, 6.0 m^2) for pre-treatment and typically either NF or low-pressure RO membranes for desalination – both UF and NF/RO modules are mounted in stainless steel pressure vessels (Inaqua PVS 4040 4″ 600 psi). The 4″ vessels allow an facile interchange with compatible membrane modules. The system is equipped with a backwash option for the UF membrane (not the subject of this work) via a bladder tank (Refix DD 25, Reflex Winkelmann, Germany). The bladder tank can be charged with UF permeate with a pressure of up to 10 bar and a maximum useful volume of 18.7 L, providing a discharge pressure of 4 bar for backwashing. For this purpose, a check valve (HP-Rückschlagventil SS 316/FKM, MHK, Germany) is installed in the feed line to ensure water flow from the bladder tank toward the UF membrane during backwashing. Additionally, one normally open (NO) solenoid valve (A3523/0804/1802-NO 24 V-DC, Busch Jost, Germany), one normally closed (NC) solenoid valve (A3523/0804/1802-NG 24 V-DC, Busch Jost, Germany), and one NC solenoid valve with backpressure (2/918–69/0804/R270-GD-2E 24 V-DC, Busch Jost, Germany) are integrated to enable rapid and reliable switching for flow control during the backwash operation. The system can also be reconfigured to enable osmotic backwashing of the NF/RO membrane using an 8 L (Tanksdirekt, Germany) installed in NF/RO permeate line.

In the present work: i) the UF pre-treatment was replaced with a 1 μm polypropylene (PP) cartridge filter with a 10″ stainless steel housing (both from Wolftechnik Filtersysteme GmbH, Germany), to minimise U adsorption; and ii) four 4" NF membranes experimented with, specifically three from Nitto Hydranautics – HydraCoRe50 (HY50), HydraCoRe70 (HY70) – and as well as NF90 and NF270 (DuPont Filmtec, 7.6 m^2). Characteristics of the NF membranes are summarised in Table S7. It must be noted here that the Hydracore membranes have been added for potential surface water applications (future field studies using this mobile laboratory) where organic matter is a major contaminant. The cartridge filter showed a maximum pressure drop of 0.4 bar in the PV-membrane system when operated at a 5-bar setpoint (Fig. S31).

2.5. Power supply and energy storage options

For powering the most important electrical load in the system – the helical rotary pump – two options are available. Firstly, the trailer has 600 W of PV modules (Offgridtec PCB-ETFE 100 W 39 V semi-flexible solar panel) that are connected in a 3-series / 2-parallel configuration to achieve a maximum power output of 600 W and a maximum voltage of 117 V_{DC}. This setup is necessary to provide sufficient voltage and power to drive the helical rotary pump. When reaching the desired field-trip location, the side of the trailer visible in Fig. 1 should face south (in the northern hemisphere) in an unshaded position and the PV array (mounted on an aluminium frame) should be tilted to nominally match the latitude angle, which typically gives the best year-around performance. Secondly, the trailer is equipped with a solar array simulator (SAS, Chroma 62050H- 600S, Taiwan) that is able to emulate the output of the PV array using pre-recorded solar irradiance (SI) temperature data from the rear-side temperature of the PV panels. The advantage of the SAS is that it allows for the same "solar day" to be repeated. This is especially useful when wanting to compare the performance of different NF membranes with a water source in one location and a variation with available solar irradiance (SI) is not desired. Most efficient use of the available PV power output is enabled via the use of a maximum power point tracker (MPPT) charge controller (Victron Energy MPPT 150/70-Tr). The charge controller has a maximum input voltage of 150 V_{DC} and 48 V_{DC} output, the latter designed to be compatible with 48 V energy storage systems. For all experiments where electrical energy storage is needed to buffer fluctuations in the available SI or during longer periods of intermittency (e.g. dark clouds, nighttime) two different technologies are available: i) lithium iron phosphate batteries (PowerBrick+; 48 V_{DC}, 50 Ah, 2400 Wh) as well as ii) a more novel supercapacitor (SC) module (Sirius, KilowattLabs; 48 V_{DC}, 2500 Wh). The charging/discharging of both of these storage components is realised via the MPPT charge controller. Supercapacitors represent the next generation of energy buffering technologies that are starting to compete with lithium batteries [27], also for in the renewable energy sector [28].

For providing power to all auxiliary electrical loads – this includes the PLC, sensors, lighting, as well as charging laptops and mobile phones while undertaking field-work – a further 200 W of PV panels are mounted on one trailer door (plus 400 W as a roof extension) and a 24 V_{DC} battery bank (PowerBrick+ LFP 50 Ah, 1200 Wh) is included.

2.6. Set-point determination with variable water salinity and recovery

Before each experiment, a 'set-point' – the position of the back pressure valve on the concentrate stream, which is set to create the desired transmembrane pressure (TMP) – is defined. The set-point is specific for each system configuration as it is impacted by the amount of power available, the feedwater salinity, the selected membrane, and pump characteristics. Selecting a set-point (e.g. 8 bar) at a chosen power (600 W) not only provides a reference point for each experiment (e.g. comparing the performance of different membranes), but also impacts on the system performance. Since the maximum power available now corresponds to a maximum operating TMP, this effectively places an upper limit on the TMP achievable and establishes an operating range for the PV-membrane system under variable operating conditions. This then impacts on the key performance indicators influenced by the set-point include system recovery, permeate quality, and SEC, as detailed below:

System recovery and feed salinity: System recovery refers to the ratio of permeate water to feedwater volume. Higher recoveries are generally desirable because they increase the volume of clean water and reduce concentrate volume. However, as feed salinity increases, the osmotic pressure also increases, demanding more hydraulic pressure to achieve the same flux. Operating at a set-point of high recovery under high salinity conditions however can increase the risk of membrane fouling or scaling [29,30]. Instead, operating at low recovery may enable the concentrate to be used for secondary applications and thus avoiding further treatment. Thus, for brackish feedwater, a moderate recovery target – typically about 25 % – is chosen [30,31].

Production quality and feed salinity: The selection of set-point can directly impact permeate quality, especially under varying feed salinity conditions. As feed salinity increases, the osmotic pressure of the feedwater also increases, thus to maintain a positive net driving pressure across the membrane (which is necessary for water to permeate) the applied pressure (set-point) must increase proportionally [32]. Concentration polarization will increase the osmotic pressure at the membrane surface and this will further reduce the effective TMP.

Specific energy consumption and feed salinity: The SEC (kWh/m^3) is the amount of energy (kWh) consumed per cubic meter (m^3) of permeate produced, while the inverse SEC (m^3/kWh) reflects the productivity per unit electricity. Since this is dependent on the operating pressure and flow conditions, the SEC can be directly affected by the set-point. At a higher salinity, there is increase in TMP which can necessitate an increase energy demand from the pump [33]. In such cases, maintaining a previously set recovery set-point could the increase SEC. Therefore, optimizing the set-point with respect to both current salinity and membrane characteristics is essential for minimising SEC while maintaining acceptable performance.

Set-point methodology: A series of experiments were conducted, aimed to assess how variations in operating set-point influence the system performance across different salinities and membrane types. This relies on the set-point methodology adapted from Richards et al. [34], summarised below with more a detailed step-by-step guide provided in Section S2 of the Supplementary Information. The SAS was used to emulate the real-world characteristics of the PV array. For set-point experiments, the SAS settings were selected to match Standard Test Conditions (STC ≡ a fixed SI of 1000 W/m^2 and PV module temperature of 25 °C), thus producing 600 W. This enabled the pump to receive constant input power from the SAS and achieve the maximum feed flow rate of 600 L/h from the pump. It should be noted that the NF modules are being operated at significantly less than the maximum feed flow rate of 3600 L/h [30,31], which reduces crossflow velocity and may exacerbate concentration polarization. Then, the system performance – defined in terms of permeate flux, EC retention, and SEC – is then mapped out at different set-points (TMPs of 5, 6, 7, 8, 9, 10, 11, 12 bar) was investigated over a wide range of salinities for the selected membranes as a function of pressure. For this, NaCl of general-purpose grade (VWR, Germany) was diluted in deionised water (pH 6.1, 0.1 μS/cm) to prepare the feed solutions with NaCl concentrations of 1, 2.5, 5, 7.5 and 10 g/L. The selection of the set-point is based on the resultant recovery that was chosen to be <30 %, which is in line for maximising the operational lifetime of the NF membranes [30,31]. Subsequently, to determine the limits of the PV-membrane system, a much higher NaCl concentration of 20 g/L was tested, for which two higher set-points of 14 and 20 bar were used.

2.7. Safe-operating window (SOW)

The performance information gained from the brackish water set-point experiments above are important in determining an optimal operating set-point to maximise the system performance, by identifying the operational constraints that can allow the system to operate within a SOW [17,34]. The SOW is the defined set of limits for key process parameters within which the membrane module and system can operate while maintaining: i) desired permeate quality; ii) sustainable flux (i.e. minimising scaling and/or fouling); iii) membrane integrity; and could also be extended to comply with iv) an acceptable cleaning frequency as well as v) the membrane manufacturer's warranty. An example of the SOW is illustrated in Fig. 3, determined via mapping out the operating constraints, embodying the hydraulic, electrical, and membrane-performance characteristics of the PV-membrane system, which are detailed as follows: i) the minimum pump power to overcome osmotic pressure and produce a permeate flow. However, this constraint is usually superceded by: ii) the minimum retention that is required to attain drinkable permeate. Constraints iii) and iv) are defined by the minimum and maximum pressure set-points achievable with the system, respectively, while v) is the maximum desired recovery (e.g. to avoid scaling) and vi) is constrained by the maximum electricity consumption of the pump. It should be noted that temperature and pH were not considered in the SOW determination here.

For autonomous operation, the SOW for the PV-membrane system defines the operational limits, within which the system can both operate and also produce clean drinking water that meets the chosen standard

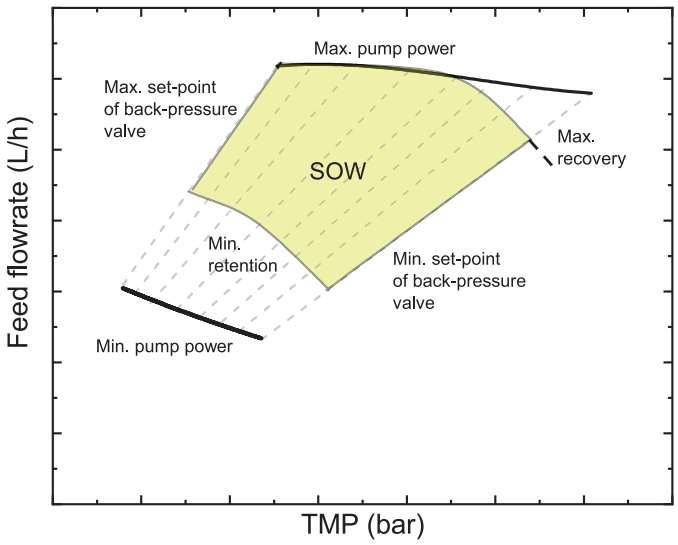

Fig. 3. Graph outlining the boundary conditions of the experimentally-determined safe operating window (SOW) of a PV-membrane system as a function of transmembrane pressure (TMP) and feed flowrate. The constraints from the following factors define the SOW: i) the minimum pump power required to produce a permeate flow; ii) the minimum retention that is required to attain drinkable permeate; iii) the minimum pressure set-points achievable with the system; iv) the maximum pressure set-points achievable with the system; v) maximum desired recovery; and vi) maximum electricity consumption of the pump – as discussed in detail in the main text.

and remain within the recommended limits for minimising scaling/fouling. The SOW was originally theoretically proposed by Feron for wind-powered membrane filtration systems [35] and expanded upon experimentally [17,34], but neither for PV-membrane systems nor over a wider salinity range. In addition, previous research assumed that if permeate was produced then the water must meet the drinking guideline values, which is not strictly true when the amount of PV power available varies contunuously. In this work, a total dissolved solids (TDS) value of 1 g/L was selected as the desired water quality target. Thus, any operating condition inside the highlighted SOW (Fig. 3) – for any particular combination of salinity and membrane choice – is regarded as safe drinking water. The method for mapping out the SOW for the PV-membrane system was adopted from earlier experimental work applied to wind-membrane systems [34]. It is worth noting that while the SOW concept is applicable to any pressure-driven membrane system, it needs to be appreciated that by changing any of the following parameters – feedwater salinity, pump type, pump motor, or the membrane – will impact on the SOW. In this work, the feedwater salinity and the membrane type were varied and the resulting SOW are reported in Sections 3.2 and 3.3, along with Section S9 in the Supplementary Information.

2.8. Solar day choice for direct coupling and energy buffering

For solar day experiments, previously measured SI data from one day (26 May 2016) at the KIT Solar Park in Karlsruhe, Germany was collected from sunrise to sunset at 1 s resolution. This partly cloudy day (Fig. 4A) was chosen as i) there is typically a high amount of SI available, and ii) passing clouds cause eight fluctuations near midday (Fig. 4B), resulting in large drops in the availability of PV power, which, in turn, will challenge the hydraulic performance of the system [36]. Note, the temperature plotted in Fig. 4A is not the ambient air temperature – it is the measured temperature on the rear-side of the silicon PV modules installed in the KIT Solar Park [37].

Two operation modes characterized these experiments, i) directly-connected and ii) energy buffering.

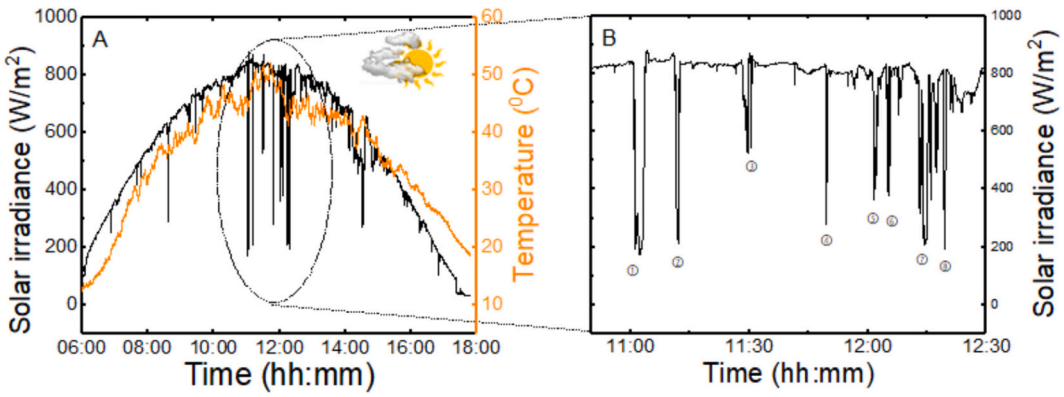

Fig. 4. (A) Measured solar irradiance (SI) and rear-side PV module temperature data of the partly solar day which exhibit (B) eight abrupt SI fluctuations in the middle of the day (data taken from KIT Solar Park on 26 May 2016, Karlsruhe, Germany).

The option of using SCs for energy buffering will be investigated using two NF membranes with different permeabilities: NF270 and HY50. This investigation aims to determine how membrane selection affects PV energy utilization by the SC module. Additionally, during buffering operation, the charge-discharge characteristics of the SC module, the SEC, and the quality of the permeate produced (measured in terms of EC) – will be monitored.

2.9. Water source and water quality analysis

For these experiments, a real water source with a challenging naturally-occurring contaminant, uranium (U), was located near the Krunkelbach Pit in Menzenschwand region of south-west Germany, as shown in Fig. S4. The Krunkelbach Pit in the Menzenschwand area was renowned for its exploration and utilization of uranium reserves [38]. For the PV-membrane experiments conducted here, about 1000 L was collected from a location nicknamed 'Waterfall' (Coordinates: N 47°50.317′ E008°02.812′). The water quality data is provided in Table S9, indicating a very low salinity and a typical U concentrating of ~60 µg/L, which is twice the WHO guideline value [39]. The experimental design for these solar day experiments is summarised in Table S8.

In addition to the inline water quality sensing, samples were taken periodically for further analysis. Inductively coupled plasma mass spectrometry (ICP-MS, 7900, Agilent, Japan) was employed for multi-element analysis, including uranium (see Table S9). For this, a standard reference (ICP standard solution VI 30 elements, 9.9 ± 0.5 mg/L of U, Certipur®, Germany) was used for calibration. The limit of detection (LoD) for the U analysis was determined to be 0.5 µg/L, and a recovery test was performed as detailed in Fig. S5. For permeate sampling for U monitoring (samples for ICP-MS analysis), a sample every 15 min during the 12-h solar day (48 samples). In addition, one sample was taken every 30 s during the period with fluctuating SI during the middle of the day (~90 min; equivalent to 180 samples). The pH and EC were measured using a multi-parameter portable meter (WTW ProfiLine pH/Con 3320, Germany) with waterproof electrode SenTix™ pH-Electrode (0–14, 3 mol/L KCl, Ag^+ free, WTW, Germany) for pH measurements and TetraConc® 325 (1 µS/cm – 2 S/cm, cell constant 0.475/cm, WTW, Germany) for EC measurements. The multi-parameter portable meter was also used to verify the EC and pH readings from the sensors of the PV-membrane system. All experiments with U-containing water were conducted under KIT safety guidelines, with liquid waste below exemption limits (1 Bq/g [40], ~45 mg/L U), and standard laboratory and waste management procedures were strictly followed.

3. Results and discussion

Each system has intrinsic performance characteristics due to the individual design. For this reason the novel mobile laboratory will be characterized in detail prior to the example application for low salinity groundwater containing uranium.

3.1. Performance of PV-membrane system under different set-point operating pressures

An example of varying the set-point operating pressure on the PV-membrane performance is illustrated in Fig. 5. Different set-points (selected pressures between 5 and 12 bars at a maximum flow rate of 600 L/h) were investigated initially at 5 g/L NaCl for the four different NF membrane types (NF90, NF270, HY70, HY50) and plotted as a function of TMP. The pump power electrical consumption rises with increase in pressure (Fig. 5A). This is to be expected as the hydraulic power – defined as the product of the flowrate and pressure – is also rising. The feed flowrate increased linearly with rising TMP (Fig. 5B), with the highest flowrates of 600 L/h still being able to be maintained by the pump even at high TMPs. This result contrasts with earlier published results using a helical rotary pump from another manufacturer (NOV/Mono Pumps), where the feed flow steadily reduced as the TMP increasedRichards et al. (2014) [34]. This was likely due to the lower power (300 W) motor used in the earlier work, compared to the 500 W maximum observed here (Grundfos pump). The flux – defined as the permeate flow rate divided by the membrane area – commenced after the osmotic pressure (~2.1 bar for 5 g/L NaCl) was overcome (Fig. 5C).

The flux varied little with the operating point as this is primarily a function of the intrinsic permeability of a chosen membrane. As the TMP rises the flux increases from ~2 L/m^2.h (the minimum that can be read out from the permeate sensor) to ~42 L/m^2.h at a TMP of 12 bar. The recovery – defined as the volumetric fraction of permeate produced – increased steadily as a function of TMP, with values over 8 bar exceeding the desired 30 % limit (Fig. 5D). To reach the 1 g/L TDS target value with 5 g/L feedwater, a retention of 80 % is required. This is achieved for all set-point values; at the minimum set-point, a TMP of about ≥4 bar is required to achieve the desired retention of about 80 % for 5 g/L concentration (Fig. 5E). The TMP demand to realise this retention increases gradually as the set-point increases and a maximum retention of >90 % can be achieved. When it comes to SEC (Fig. 5F), it can be seen that higher set-points yield a lower SEC (as low as 1.5 kWh/m^3 for a set-point of 12 bar) and that beyond a TMP of 8 bar the SEC value plateaus for each of the set-point values. Fig. 5G demonstrates that at higher set-point pressures (e.g. 11–12 bar), the permeate EC is excellent, remaining within the target value of 1.1 mS/cm down to 6 bar. Prdictably, at lower set-point pressures (e.g. 6 bar) the system will not often have enough power and will typically operate in the 2–4 bar range where the permeate quality is poor. Finally, Fig. 5H demonstrates a new figure-of-merit – the inverse SEC – clearly showing that under the best operating conditions (12 bar set-point) a value of 0.6 m^3/kWh can be achieved, but drops to only one-third of this at low set-point pressures.

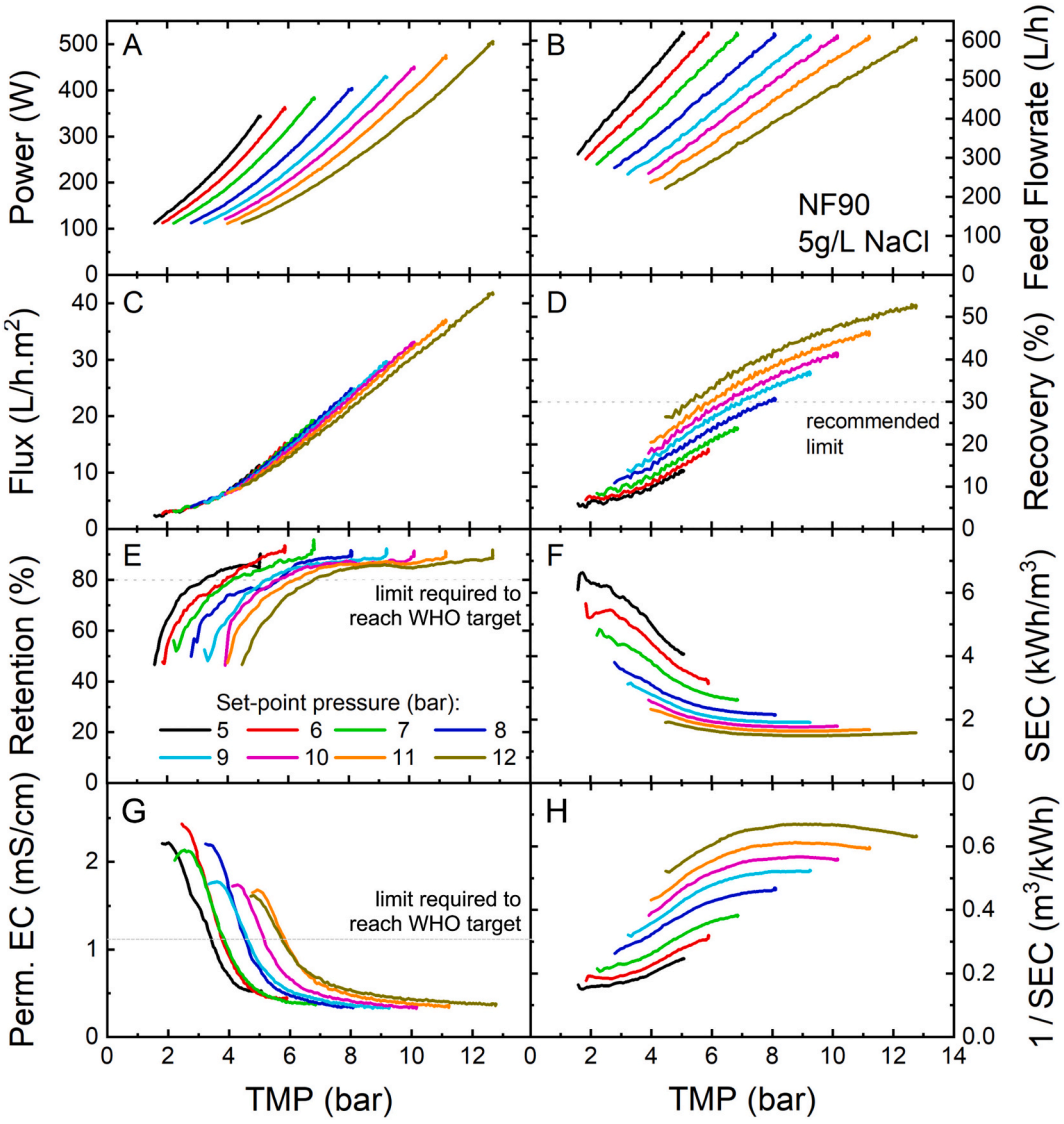

Fig. 5. Steady-state performance of the PV-membrane system operated over the set-point range of 5–12 bar (NF90, 5 g/L NaCl, feedwater temperature 22 °C ± 1.5 °C): (A) pump power, (B) feed flowrate, (C) flux, (D) recovery, (E) retention, (F) SEC; (G) permeate electrical conductivity; and (H) inverse SEC. In (E) and (G) the required retention and permeate EC limits, respectively, to achieve the desired WHO target are also plotted, while the 30 % upper limit on recovery in shown in (G).

The performance of the PV-membrane system for desalinating 5 g/L feedwater equipped with the three other NF membranes (NF270, HY50, HY70) is given in Figs. S6–S8. These were investigated under the same set-points, and the pump attained the maximum feed flow (600 L/h) during each test condition. However, membrane performance showed variations, with the main concern being that the maximum retention achieved was below the requirement to produce drinkable water for these three membranes, and this not producing potable water. This is due to the salt retention characteristics of these membranes (NF270, HY50, HY70), which limit desalination performance to feed salinities below 5 g/L. The low salt retention observed is primarily attributed to the higher molecular weight cut-off (MWCO) – or larger effective pore size – compared with the tighter NF membrane (NF90), leading to reduced size exclusion, as commonly known for NF membranes with larger pores [41]. In addition, surface-charge screening at high ionic strength diminishes electrostatic repulsion, further lowering salt retention [42]. The choice of NaCl to characterize a system that is applied to low salinity water with more complex contaminants bears limitations that require further consideration. Thus, a SOW is not achievable under these performance conditions for the 5 g/L concentration (and above).

Subsequently, the feedwater salinity was varied to lower values (1 g/L and 2.5 g/L) and then higher values (7.5 g/L and 10 g/L) for all four NF membranes, with all performance maps being supplied in the Supplementary Information (Figs. S9–S24). For a feed salinity of 1 g/L, naturally all membranes produced drinkable permeate regardless of the retention levels, since the target permeate salinity is also 1 g/L. The performance covers most surface and low salinity groundwaters, where typically other contaminants than NaCl are of concern, as illustrated at the example later. At a feed salinity of 2.5 g/L, a minimum retention of 40 % is required to achieve the target permeate quality. This level of retention was achieved only by the NF90 and NF270 membranes, whereas the HY50 and HY70 membranes fell below this threshold. This indicates that only some NF membranes can operate within a SOW at this feed salinity.

Finally, the performance maps at the highest TDS concentration of 20 g/L were determined experimented with the NF90 membrane only at the 14 bar and 20 bar set-points (Figs. S25 – S26). The high TMP operation will improve the retention of the NF membrane at high feed salinity (20 g/L) where the effective TMP is reduced by the high osmotic pressure and diffusive transport reduces the observed retention. For this feed salinity, a minimum retention of 95 % is needed to realise a permeate of about 1 g/L. However, for both TMP up to 20 bar, the

permeate quality is not drinkable with this NF membrane. This indicates that this salinity is outside the limits of this system.

3.2. Safe operating window of PV-membrane system when treating 5 g/L feedwater

All of the performance mapping data in Fig. 5 (NF90) along with Figs. S6–S8 (for NF270, HY70, HY50 respectively) was then used to create the SOW plot for treating 5 g/L feedwater as shown in Fig. 6. For each membrane, the SOW is realised by plotting the feed flowrate against the TMP with the constant set-point values (5–12 bar) marked as dashed lines. Other key parameters that define the SOW are also plotted (e.g. recovery and pump power limits) while other indicators (flux, retention, SEC) are indicated as well.

For the NF90 membrane (Fig. 6A), it can be seen that the limiting factors that define the SOW in this case are primarily the pump power (both minimum and maximum) and the maximum desirable recovery of 30 %. There is a possibility of increased water production at higher recoveries – in other words a larger SOW would be possible – however, higher recoveries come with a higher risk of scaling, especially at the comparatively low crossflow velocities. The minimum retention of 80 % required to produce safe drinking water that meets the desired 1 g/L target value (from 5 g/L feed salinity) is realised at minimum SEC of 3.0 kWh/m^3. The water quality was achieved across all the investigated operating set-points of 5–12 bar, making this set-point ideal for treating 5 g/L feed salinity with the NF90 membrane.

In terms of the other membranes, the NF270 membrane (Fig. 6B) displayed a different performance profile with a lower retention of approximately 55 % and a maximum recovery also around 55 % across the set-points investigated. Although a low SEC of about 1.5 kWh/m^3, was achieved at high set-point, notably due to the low retention, the permeate produced across all the set-points is not suitable for drinking, and thus a SOW of the membrane for 5 g/L feed salinity cannot be mapped out. The retention of HY70 was even lower at around 25 %, while the maximum recovery increased to approximately 15 %, the flux remained low at 10 L/m^2.h, and the SEC increased to about 4.0 kWh/m^3 (Fig. 6C). Inevitably, no SOW could be achieved for this membrane within the investigated operating set-points up to 12 bar. The lowest retention performance is observed with HY50 membrane over the same operating set-point range as shown Fig. 6D. This exhibited a reduced retention of about 20 % across all the set-points. Although, a desirable recovery of 30 % (increased flux compared to HY70), was realised at low SEC of 2.0 kWh/m^3, however, the quality of permeate produced across these set-points is not be suitable for drinking. This makes the SOW for treating brackish water of feed salinity of 5 g/L impossible with this membrane, and thus no ideal set-point can be recommended. It should be noted here that the membranes are evaluated in light of the relevance for surface water treatment, notably organic matter removal. The investigations at brackish water salinities serve as an example for a case where a SOW cannot be achieved.

3.3. Safe operating window of PV-membrane system operation at different salinities

The SOW of PV-membrane system operation depends strongly on the feedwater salinity as this can directly influence the retention of the membrane. The SOWs of the PV-membrane system using NF90 membrane at different feed salinities 1, 2.5, 7.5 and 10 g/L are plotted in Fig. 7. As indicated above, at low feed salinity of 1 g/L (Fig. 7A), a SOW for drinkable permeate is achieved as the feed salinity is already within the palatable salinity of drinkable water. When the feed salinity increases to 2.5 g/L (Fig. 7B), a minimum retention of 60 % is required by the system to attain the palatable limit. At both of these low concentrations it can be seen that the desired maximum recovery of 30 % is a key limiting factor. The size of the SOW region reduces as the salinity increased to 7.5 g/L (Fig. 7C), where a minimum retention of 87 % is

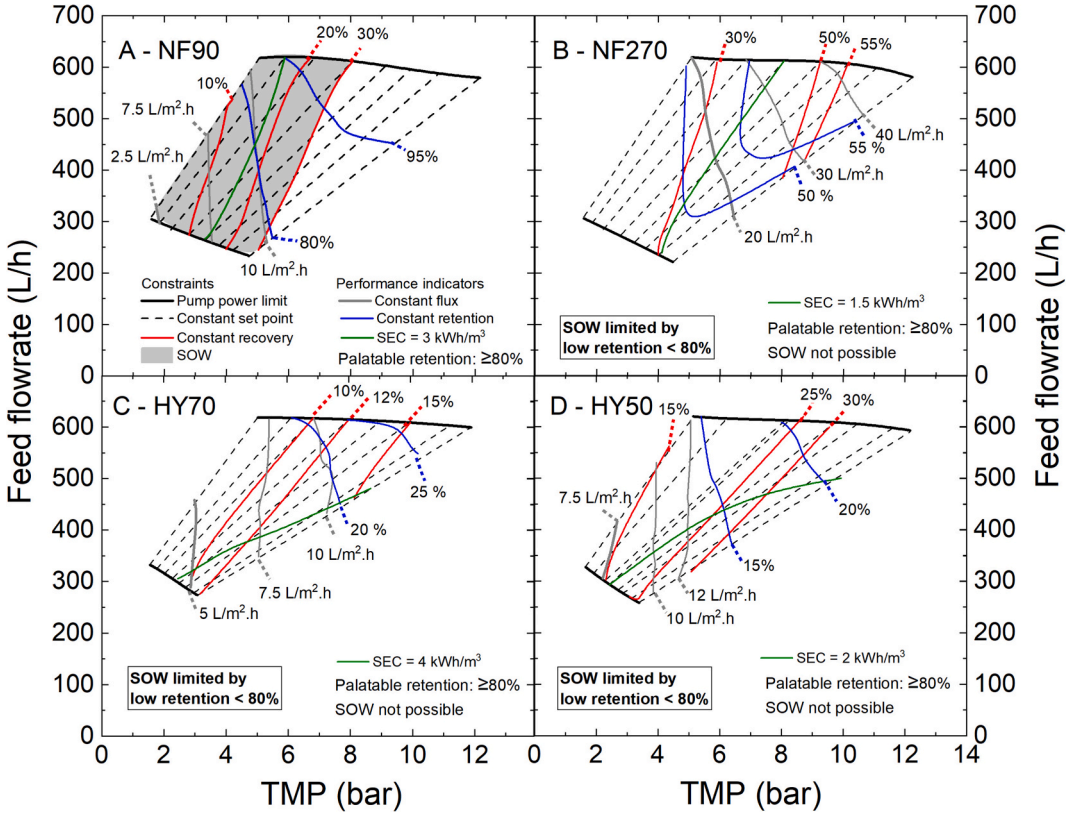

Fig. 6. Safe operating windows that were mapped out for the PV-membrane system operated over the set-point range of 5–12 bar and equipped with different NF membranes using brackish feedwater with a salinity of 5 g/L NaCl (feed temperature 22 °C ± 1.5 °C). (A) NF90, (B) NF270, (C) HY70 (D) HY50.

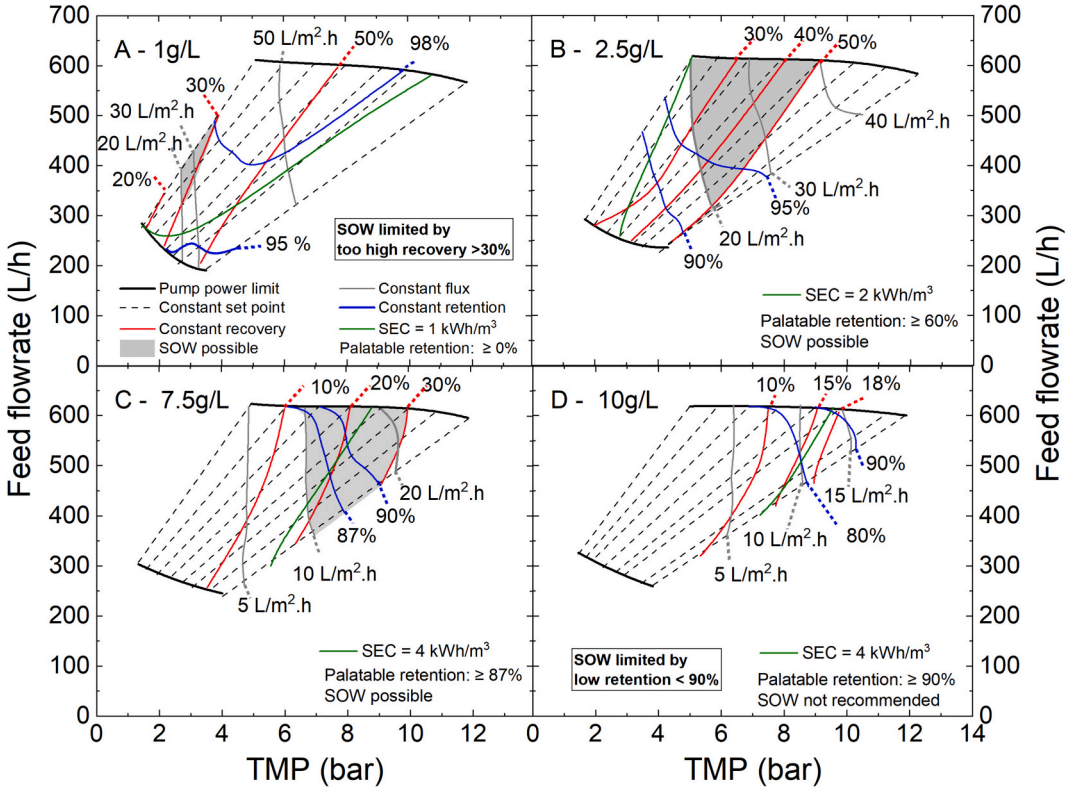

Fig. 7. Safe operating windows that were mapped out for the PV-membrane system operated over the set-point range of 5–12 bar and equipped with NF90 membrane using a range of brackish feedwater salinities (feed temperature 22 °C ± 1.5 °C). (A) 1.0, (B) 2.5, (C) 7.5, and (D) 10.0 g/L NaCl.

required to produce drinkable permeate. In Fig. 7D, no SOW could be realised at 10 g/L using the NF90 membrane. This is because the retention across all the set-points is below the desired 90 % value required to achieve drinking water that meets the palatable limit. Altogether, the results shown in Fig. 7 highlight the importance of matching the correct membrane to the feedwater quality.

To determine the set-point role in limiting the performance at high salinities, the PV-membrane system was now tested using the NF90 membrane to in treat feedwater with 20 g/L salinity. A set-point of 14 bar was mistakenly used at the beginning, which is less than the osmotic pressure of the feedwater (about 15.5 bar) that needs to be overcome. Thus, the performance at this setting (Fig. 8A) is poor – both the recovery and retention are very low, meaning that although some permeate is produced this is brackish. When the set-point was increased to 20 bar (Fig. 8B), the performance improves markedly, with flux, recovery and retention all increasing significantly and the SEC decreasing markedly. Although the maximum retention of 83 % fell just short of the 90 % required to meet the 1 g/L permeate salinity target, this experiment demonstrates the value of choosing the correct set-point. As the pump and all of the sensors in the PV-membrane system are limited to 20 bar maximum operating pressure it was not possible to go to a higher set-point in order to realise a SOW at this salinity.

Given the relatively poor performance of the looser NF membranes (NF270, HY70, HY50) for treating water with salinities higher than 1 g/

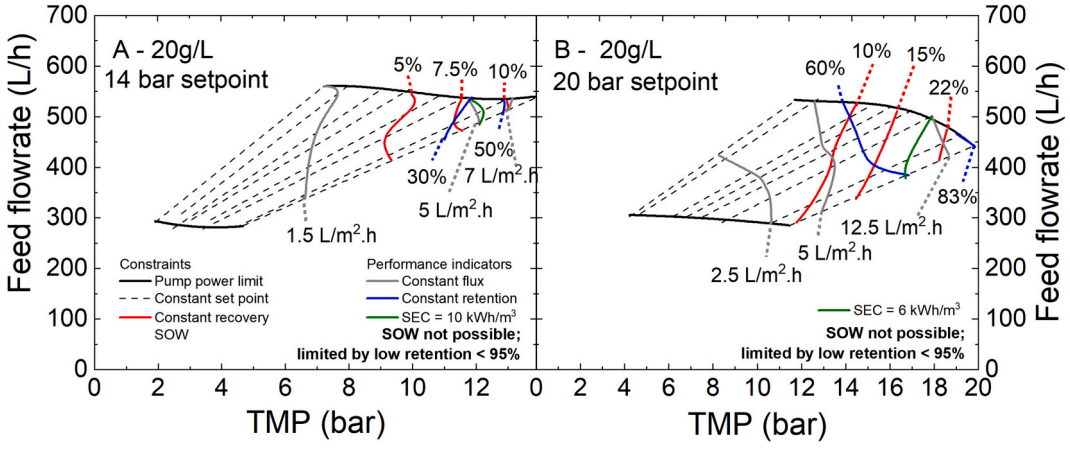

Fig. 8. Safe operating windows that were mapped out for the PV-membrane system equipped with NF90 membrane using brackish feedwater with a salinity of 20 g/L NaCl (feed temperature 22 °C ± 1.5 °C) and operated at the maximum set-points of: (A) 14 bar, (B) 20 bar.

L, these SOW results are provided only in the Supplementary Information (Figs. S27–S29). Overall, increasing the salinity reduced the flux, recovery and retention, while the SEC increased. Typically, the salt retention was too poor and the resulting permeate did not meet the 1 g/L target value. Indeed, a maximum recovery of 30 % – recommended for an operational lifetime of 1–2 years for membranes [30,31] – was achieved at TMP ≤5 bar only for the 1 g/L feedwater salinity.

3.4. System performance over a solar day for treatment of groundwater containing uranium

The SOW studies above revealed that for the low salinity feedwater of 1 g/L, a set-point of 5 bar was recommended for operating the PV-membrane system using the different NF membranes. In the following section, natural groundwater contaminated with uranium and

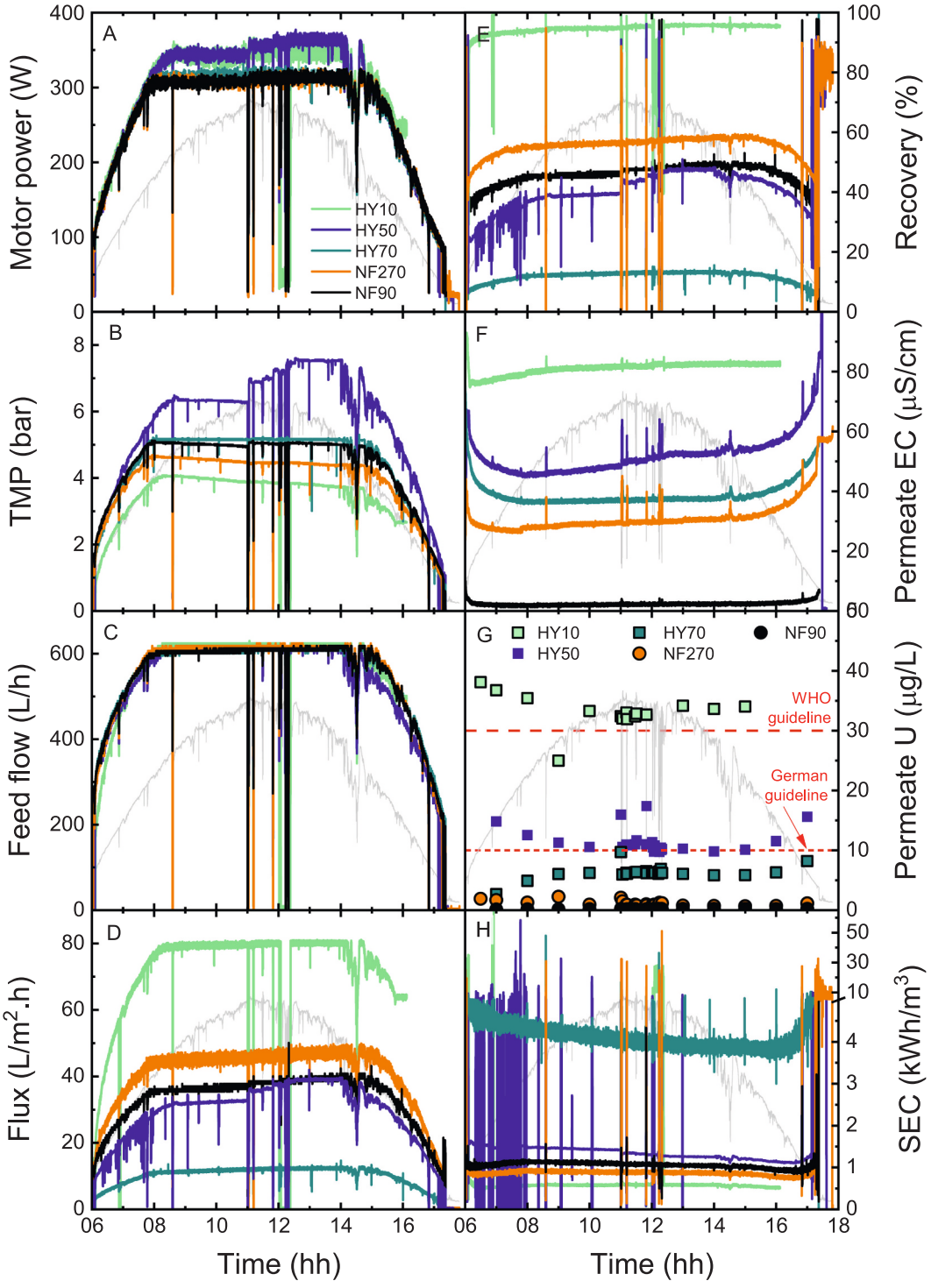

Fig. 9. Solar day experiments were conducted using the PV-membrane system equipped with different NF membrane types to treat Menzenschwand water (set-point 5 bar, 50 ± 5 µgU/L, pH 7.5 ± 0.4, EC 83 ± 9 µS/cm, TDS 42 mg/L, 17–32 °C): (A) motor power, (B) TMP, (C) feed flow, (D) flux, (E) recovery (F) permeate EC, (G) permeate uranium concentration and (H) SEC. The WHO (red dashed line) and German (red dotted line) guideline values for the uranium concentration in drinking water are also plotted in (G).

exhibiting low salinity (TDS < 0.1 g/L) was treated with the PV-membrane over the course of one "solar day" (sunrise to sunset). To evaluate the PV-membrane system performance with different NF membranes under the selected set-point conditions (5 bars at optimum PV conditions of 1000 W/m^2 and 25 °C), Menzenschwand water was treated on this solar day. The solar day – which relies on pre-recorded SI data – can be repeated in the field, thanks to the SAS. Without this, the constantly changing weather would render it impossible to achieve any meaningful comparison between the four membranes, for which 11 h is required for each experiment (not including set-up time).

The key performance parameters investigated were hydrodynamics (TMP, flow rates, flux), recovery, SEC, and permeate water quality (both as TDS as well as U concentration) – as plotted in Fig. 9, against the backdrop of the solar irradiance (taken from Fig. 4A). Additional supplementary data – including the daily cumulative permeate production, water permeability, feedwater temperature, feed and permeate pH, as well as EC retention – are reported in Fig. S30. It can be seen that the motor power (Fig. 9A) and hydrodynamics (feed flowrate and TMP shown in Fig. 9B and Fig. 9C, respectively) mimicked the solar day – including the fluctuations in the middle of the day – regardless of the membrane type. The observed flux and SEC (Fig. 9D, H) were proportional to membrane permeability (Table S7). The obtained SEC of NF, which varied from 1 to 4 kWh/m^3 during maximum power input during the solar day, could be higher than the minimal energy input required for conventional technologies, such as ion exchange, adsorption, and chemical precipitation, in particular seeing the very low concentrations of this water that merely served as an example application in this work. However, these conventional methods regularly require regeneration, chemicals, skilled operation, and reliable supply chains, which are limiting factors for remote applications compared to the PV-membrane system. In addition, NF membranes can achieve a uranium removal of ≥95 %, such as in the case of PV-membrane operated with NF90 at ~35 L/m^2.h and with ~1 kWh/m^3 SEC, which is very comparable to previously mentioned conventional methods [43], while powering the system with PV enables fully off-grid treatment.

In terms of water quality, permeate EC (Fig. 9F) and uranium in the permeate (Fig. 9G) followed the salt retention characteristics of the membranes. Three membranes – NF270, NF90, and HY70 – achieved both the German and WHO guidelines for uranium in drinking water. In contrast, the results achieved for HY50 lay just above the German guideline. From Fig. 9F it should be noted that the the permeate EC quality remains relatively stable for a large fraction of the day, roughly from 7:00 to 17:00. This is despite the large fluctuations during the middle of the day and regardless of membrane choice. Outside the aforementioned time window the level of solar irradiance is too low (< 250 W/m^2), then the electrical power availability limits the system not produce enough power to maintain the same permeate EC as during the middle of the day. In particular, U removal was dependent on the membrane molecular weight cut-off (MWCO) (or pore size): tighter NF membrane (NF90) with the lowest MWCO (90–180 Da) achieved low U concentration in the permeate, while the NF membrane with the highest MWCO (HY10, 3000 Da) exhibited high U concentration in the permeate. This observation supports the important role of size exclusion in the separation mechanisms for U removal by NF, as previously reported [44,45]. The recovery (Fig. 9E), in particular, which is linked to the selected SOW, was higher than 30 % for NF270, NF90, and HY50, while HY70 was below 30 % and hence within the SOW. The impact of the energy fluctuations on water quality during PV-membrane system operation to treat Menzenschwand water was investigated in detail in the following section.

3.5. Uranium removal with PV-membrane system during solar irradiance fluctuations

To evaluate the influence of the variable operation of the PV-membrane system on U removal from low salinity Menzenschwand water, uranium in feed, permeate, and concentrate as well as permeate EC were monitored over the solar day, with an increased number of samples being taken during the period of fluctuations (Fig. 10). The U concentration after the cartridge filter was deemed to be very similar to that in the feedwater, thus indicating negligible U adsorption. The U concentration – in the feed, permeate and concentrate – did not vary over the solar day, compared to permeate EC that increased gradually toward the end of the day (Fig. 10A). While fluctuations resulted in increased permeate EC – particularly with NF270, HY50, and HY70 – the U concentration was within the same range over the solar day including the period of fluctuations (Fig. 10A). This highlights effective removal, presumably due to size exclusion. The U concentration in the concentrate of NF270 and NF90 was higher compared to the feed, due to retention by the membrane.

For the HY50 and HY70 membranes, the U concentration in concentrate was similar to that in the feed, while the permeate U concentration was low, suggesting that adsorption may have contributed to removal. Differences in U adsorption are likely influenced by the membrane polymer materials, including both active layer and support layer materials [22], which is the subject of parallel investigations. From the energetical point of view, to maintain the same water quality in the permeate during PV-membrane system operation an energy buffering strategy to mitigate the fluctuations can be employed - this is investigated in the following section. The repeatability of the results obtained using Prototype VII are detailed in Section S12 and Fig. S32 in the Supplementary Information. The slight differences in performance (power consumption, flux, recovery, permeate EC, and SEC) are all attributed to variations in feedwater temperature (ΔT ~ 7.5 °C).

3.6. Performance of the PV-membrane system with energy buffering

Energy buffering can improve the performance of PV-NF membrane systems, especially in terms of improving salt retention and reducing the SEC caused by the fluctuations on a cloudy day. In the case of *U* retention however, the achievable improvement is bound to be minimal, as this is not affected by fluctuations. For this reason, U concentrations were not monitored for the energy buffering experiments. Nevertheless, the buffering is included for this application in order to describe the methodology that would be identical for other waters.

For the SC energy-buffering analysis on the PV–membrane system treating Menzenschwand feedwater, two membranes (NF270 and HY50) with poor retention but good recovery were selected for two main reasons: i) to investigate the potential of energy buffering to improve retention while maintaining high recovery, and ii) because NF270 has approximately twice the permeability (and therefore recovery) of HY50, making it relevant to examine how this difference influences the utilization of photovoltaic (PV) energy, particularly in relation to SC energy buffering and powering the overall system. The SC was programmed to switch in to boost the PV power supply when the PV power supply threshold ($P_{PVtresh.}$) reaches a certain limit requires to produce the permeate. This was determined ~300 W at ~5 bar TMP. At this point, the SC is activated to buffer the system performance. Buffering is enabled during the peak period of the solar day, which is prone to SI fluctuations (in this case, this happened between 07:30 and 14:30, i.e., 7 h). While the buffering time ($time_{buff.}$) remains within this set duration ($time_{set}$) duration of 7 h, and the PV power supply P_{PV} is above the maximum pump power with under SC energy supply ($P_{pumpmax}$), the SC automatically recharges via the MPPT charge controller. Otherwise, the SC discharges to compensate for low PV power supply. The SC stops buffering when the $time_{set}$ elapses or when the SC voltage (V_{sc}) reaches the minimum cut-off voltage (V_{scmin}) at about 45 V. This lower limit was not reached during the experiments, so the charge–discharge behavior was evaluated within the time boundary. The process control flow chart is shown in Fig. 11.

The results of the system investigation without SC and with SC are presented in Fig. 12. Under no-buffering conditions (Fig. 12A-E),

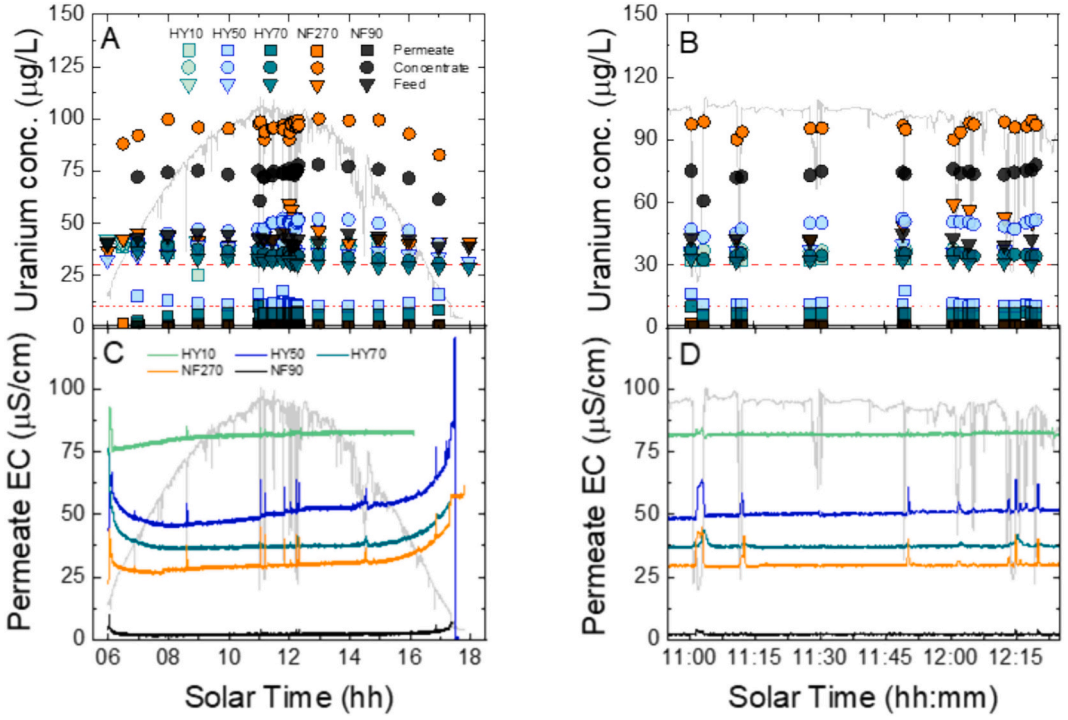

Fig. 10. Uranium concentration in feed, permeate, and concentrate during treatment of Menzenschwand water using a PV-membrane system equipped with different NF membrane types (A) as a function of solar time over the whole solar day and (B) the period of fluctuations. (C) and (D) plot the permeate EC over the same time periods, respectively (set-point 5 bar, 50 ± 5 µgU/L, pH 7.5 ± 0.4, EC 83 ± 9 µS/cm, TDS 42 mg/L, 17–32 °C): The WHO (red dashed line) and German (red dotted line) guideline values for the uranium concentration in drinking water are also plotted in (A) and (B).

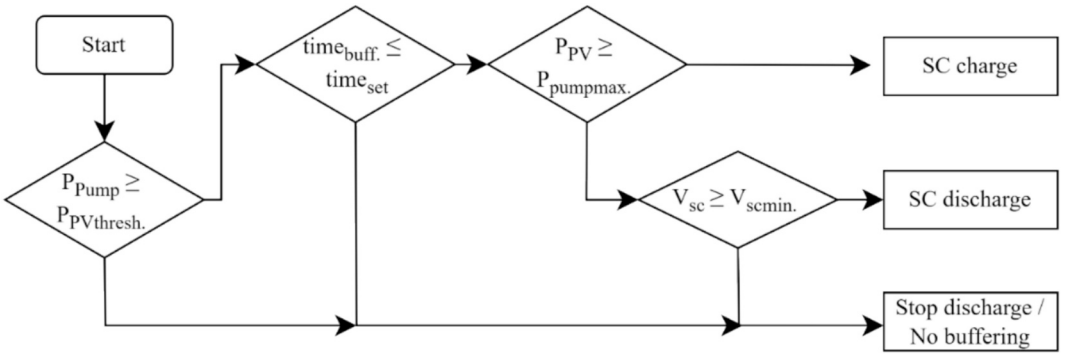

Fig. 11. Flow chart diagram of the process control of SC energy storage for buffering as implemented in the study.

representing the directly-coupled PV–membrane system, the system operated under partly cloudy SI conditions (Fig. 12A), which subjected it to noticeable SI fluctuations. The corresponding pump power consumption for both membranes was unstable for most of the solar day (Fig. 12B); however, the consumption was capped at approximately 300 W, especially for the NF270 membrane. For HY50, the power consumption was slightly higher, with a correspondingly higher TMP demand of ~6 bar compared to ~5 bar for NF270 (Fig. 12C). This behavior is expected because a membrane with lower permeability (or recovery) requires a higher TMP to achieve a given flow rate (e.g., ~600 L/h in Fig. 12D), which in turn leads to higher pump power demand. The difference in permeability between both membranes is reflected in the maximum fluxes of ~18 L/m^2.h (HY50) and ~ 38 L/m^2.h (NF270) (Fig. 12E).

With SC buffering, the system was operated under the same SI conditions and the same membrane TMP setpoint of ~5 bar for both membranes. The SC charge and discharge response to SI fluctuations and pump demand is shown in Fig. 12F. Although the SC did not charge consistently during the middle of the day, this was due to the limited extra PV power available to drive the pump and charge the SC simultaneously. Following the control algorithm described in Fig. 11, buffering was initiated once the PV power reached approximately 300 W. There was a clear increase in pump power demand under buffering (Fig. 12G) because the pump was now able to draw its full operational power, which it could not achieve under the direct-coupled configuration (without buffering). Similar to the no-buffering system, the peak power and pressure demand of HY50 (Fig. 12H) were slightly higher due to its lower permeability. Both systems maintained an approximate feed flow rate peaking at ~600 L/h (Fig. 12I), and the corresponding fluxes started at around 18 and 38 L/m^2.h and increased to approximately 20 and 42 L/m^2.h for HY50 and NF270, respectively (Fig. 12J). The steady rise in flux is attributed to the increasing feedwater temperature during the buffering period, which rose from ~20 °C to ~25 °C. The additional average performance metrics of the membranes monitored over the same 7-h period for both system configurations are summarised in Table 1.

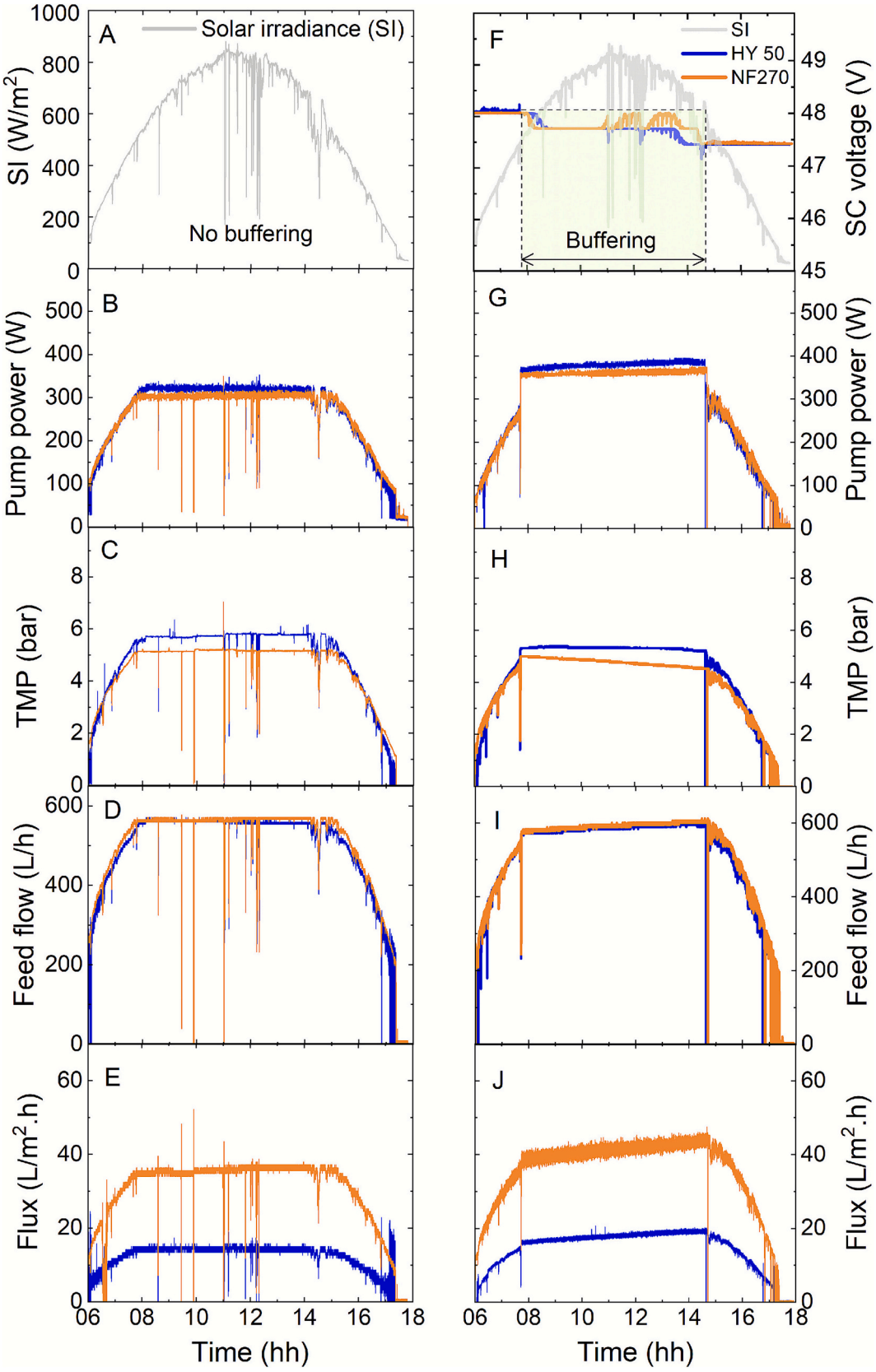

Fig. 12. Experimental investigation of energy buffering on PV-membrane system equipped with two high-permeability membranes – HY50 and NF270 – under two configurations: (left column) No energy buffering (i.e. directly coupled) and (right column) buffering using supercapacitors: (A,F) Solar irradiance and SC voltage, (B, G) Pump power, (C,H) TMP, (D,I) Feed flow, (E,J) Flux (average feed EC: ~90 μS/cm, peak permeate EC: ~30–42 μS/cm, feed temperature: 18–25 °C).

Table 1
Average membrane performance of HY50 and NF270 membranes under directly-coupled and SC buffering configurations.

Average membrane performance	HY50		NF270	
	Directly-coupled	SC buffering	Directly-coupled	SC buffering
Feed flow (L/h)	555	585	560	592
Flux (L/m^2.h)	14.3	17.9	35.3	41.3
SEC (kWh/m^3)	3.07	2.61	1.19	1.15
Recovery (%)	18.5	22.2	46.1	53.0
Retention (%)	60.4	68.5	67.2	59.4

4. Conclusions

This paper describes the design of Prototype VII of an autonomous PV-powered membrane filtration system that is mounted onto an off-road trailer such that it can be taken to remote field sites. Prototype VII brings together all of the experience gained via the design, construction and field testing on Prototypes I – VI (spanning twenty years).

Prototype VII was designed to be a mobile lab that could be towed by a four-wheel drive vehicle to remote testing sites. The design features: i) 600 W of PV panels integrated into the roof for powering the pump, while another 600 W is available for power auxiliary loads in the field; ii) the high-pressure pump can provide up to 20 bar pressure and all sensors are also rated to handle this pressure as well; iii) two pretreatment options – a 4" UF membrane and a micro-filter; iv) one 4" NF or low-pressure RO module for treatment of surface and groundwater with variable water quality challenges, in this work uranium removal from a low salinity groundwater; and v) with the option of ~2.5 kWh of both supercapacitors and lithium ion batteries for energy storage. The PV-membrane system was powered using a SAS using measured solar irradiance data. A wide range of experiments were conducted to verify the performance of the PV-membrane system when pairing five NF membranes (NF90, NF270, HY70, HY50, HY10) with different water sources – synthetic brackish feedwater with a NaCl concentration of 1 g/L up to 20 g/L.

For the autonomous operation of the PV-membrane system, the selection of a set-point operating pressure is important, limited by the pump characteristics, available power, water quality and the selected membrane. The methodology was described in detail such that this can be applied for any membrane or water. These steady-state set-point experiments were carried out using emulated solar irradiance of 1000 W/m^2 (producing 600 W of PV power) that was used to map out the SOW of each configuration, noting that the SOW definition here was now expanded to include sufficient retention as a boundary condition. HY10 did not exhibit any NaCl retention and was not investigated further for brackish water desalination (with NaCl as the chosen solute). At a 10 bar set-point for NF90 of high retention characteristics, SEC below 3 kWh/m3 was naturally achieved at low salinities (1–5 g/L), but the recommended recovery of 30 % for safe operation was only achieved at 5 g/L and an operating pressure below 6 bar. Although feedwater salinities of up to 20 g/L were attempted, the highest possible salinity that could be desalinated using NF90 was 7.5 g/L. For higher salinity feedwaters a RO membrane (such as BW30) would need to be integrated into the system, while this is usually not the case for surface or low salinity ground waters, where other contaminants are of interest. The HY50 and HY70 NF membranes exhibit limited salt retention and only exhibit satisfactory performance at the lowest NaCl salinity of 1 g/L, while NF270 was able to desalinate 2.5 g/L feedwater.

The NF membranes were applied to a real water example, in this case to remove a specific contaminant, naturally-occurring uranium,from contaminated groundwater in Menzenschwand (Black Forest, southwest Germany). Experiments were conducted over a solar day, which included large fluctuations due to passing clouds. Three membranes – NF270, NF90, and HY70 – were able to achieve both the German and WHO guidelines for uranium in drinking water with a SEC as low as 1 kWh/m^3. The remaining two NF membranes (HY10 and HY50) were not able to meet either guideline. The permeate water quality and production were not significantly affected by fluctuations, although it should be noted that inline measurement of the U concentration is not possible. Nevertheless, U concentrations in the permeate remained below the WHO guideline value, except when using the HY10 membrane. Finally, two membranes (NF270, HY50) were tested further in the PV-membrane system when supercapacitors were implemented to buffer fluctuations in solar irradiance, demonstrating the flexible design of the mobile PV-membrane system.

CRediT authorship contribution statement

Bryce S. Richards: Writing – original draft, Validation, Supervision, Resources, Project administration, Methodology, Funding acquisition, Formal analysis, Data curation, Conceptualization. **Youssef-Amine Boussouga:** Writing – original draft, Visualization, Validation, Supervision, Methodology, Investigation, Formal analysis, Data curation, Conceptualization. **Emmanuel.O. Ogunniyi:** Writing – review & editing, Visualization, Validation, Methodology, Investigation, Formal analysis, Data curation. **Andrea I. Schäfer:** Writing – review & editing, Supervision, Resources, Project administration, Methodology, Funding acquisition, Conceptualization.

Declaration of competing interest

The authors declare that they have no known competing financial interests or personal relationships that could have appeared to influence the work reported in this paper.

Acknowledgements

The Helmholtz Association is gratefully acknowledged for funding: i) the Recruitment Initiative for AIS (IAMT) and BSR (IMT); and ii) Research Field Energy – Materials and Technologies for the Energy Transition program (Topic 1 Photovoltaics and Wind Energy, 38.01.04). A special thank you to 'Team Land Rover Defender' at KIT EVM (Karl-Heinz Gräßle), as well as BMBF Bonn (Lukas Schuwerack and Johann-Josef Donau) for enabling this unconventional purchase at IAMT. The BMBF project CEWAG (FZ 03SF0575) is acknowledged for the partial funding of the PV-membrane system construction. The authors would like to acknowledge the contributions of the following people: Dr. Jochen Henkel (DuPont) for the donation of NF90 membrane; Tomas Laska (Hydranautics – Nitto) for the HydraCoRe membranes donation; Dr. Peter Berg (Inge – DuPont) for UF module provision; Lee Estrellado and Moritz Rettenmayr (IAMT) for their contribution to the system-building (planning, schematic, construction, and quotes requests and orders); Seti Frotscher (IAMT) for conducting the set-point experiments; Alexandra Moritz (IMT) for assisting with system building (facilitating access to IMT workshop, trailer modification to fit PV panels) and Land Rover maintenance support. Finally, a special thanks goes out to several of the staff at the Radon Revitalbad Menzenschwand (Germany) – including general manager Jürgen Längin and technicians Christian Seichter and Thomas Spiegelhalter – for their support with access and water collection. Open access funding was enabled by Project DEAL.

Appendix A. Supplementary data

Supplementary data to this article can be found online at https://doi.org/10.1016/j.cej.2025.172387.

Data availability

The data that support the findings of this study are available from the corresponding.

author upon reasonable request.

References

[1] United Nations, Sustinable Development Goal 6: Ensure Availability and Sustainable Management of Water and Sanitation for All, 2025 https://sdgs.un.org/goals/goal6#progress_and_info (accessed 21.11.2025).
[2] United Nations, Sustainable Development Goal 7: Ensure Access to Affordable, Reliable, Sustainable and Modern Energy for All, 2025 https://sdgs.un.org/goals/goal7#progress_and_info (accessed 21.11.2025).
[3] B.S. Richards, J. Shen, A.I. Schäfer, Water–energy nexus perspectives in the context of photovoltaic-powered decentralized water treatment systems: a tanzanian case study, Energ. Technol. 5 (7) (2017) 1112–1123.
[4] E.M. Almetwally, M.A. Elazab, A.E. Kabeel, Y. Yasser, A. Elgebaly, Solar powered reverse osmosis desalination: A systematic review of technologies, integration strategies and challenges, Desalination 615 (2025) 119228.
[5] IndustryARC, Solar Powered Water Desalination Market - Forecast (2025–2031), 2025 https://www.industryarc.com/Research/Solar-Powered-Water-Desalination-Market-801015.
[6] V.N.X. Que, D. Van Tuan, N.N. Huy, V. Le Phu, Design and performance of small-scale reverse osmosis desalination for brackish water powered by photovoltaic units: a review, in: IOP Conference Series: Earth and Environmental Science, IOP Publishing, 2021, p. 012024.
[7] S. Li, Y.-H. Cai, A.I. Schäfer, B.S. Richards, Renewable energy powered membrane technology: A review of the reliability of photovoltaic-powered membrane system components for brackish water desalination, Appl. Energy 253 (2019) 113524.
[8] WaterOnline, Colorado Company Answers Haiti's Relief Call For Clean Water, 2010 (accessed 13.06.2025), https://www.wateronline.com/doc/colorado-company-answers-haitis-relief-call-0001.
[9] SunSpring, Alternative Energy - Decentralized Microbiological Water Treatment System, 2008 (accessed 13.06.2025), https://innovativeh2o.com/wp-content/uploads/2023/08/Sunspring-Brochure-IWT-275-7.pdf.
[10] A.I. Schäfer, B.S. Richards, From concept to commercialisation: student learning in a sustainable engineering innovation project, Eur. J. Eng. Educ. 32 (2) (2007) 143–165.
[11] B.S. Richards, A.I. Schäfer, Design considerations for a solar-powered desalination system for remote communities in Australia, Desalination 144 (1–3) (2002) 193–199.
[12] B.S. Richards, A.I. Schäfer, Photovoltaic-powered desalination system for remote Australian communities, Renew. Energy 28 (13) (2003) 2013–2022.
[13] L. Masson, B.S. Richards, A.I. Schäfer, System design and performance testing of a hybrid membrane—photovltaic desalination system, Desalination 179 (1–3) (2005) 51–59.
[14] A.I. Schäfer, B.S. Richards, Testing of a hybrid membrane system for groundwater desalination in an Australian national park, Desalination 183 (1–3) (2005) 55–62.
[15] Broeckmann Schäfer, A. Richards, Renewable energy powered membrane technology. 1. Development and characterization of a photovoltaic hybrid membrane system, Environ. Sci. Technol. 41 (3) (2007) 998–1003.
[16] B. Richards, D. Capão, A. Schäfer, Renewable energy powered membrane technology. 2. The effect of energy fluctuations on performance of a photovoltaic hybrid membrane system, Environ. Sci. Technol. 42 (12) (2008) 4563–4569.
[17] B.S. Richards, G.L. Park, T. Pietzsch, A.I. Schäfer, Renewable energy powered membrane technology: Brackish water desalination system operated using real wind fluctuations and energy buffering, J. Membr. Sci. 468 (2014) 224–232.
[18] A.I. Schäfer, J. Shen, B.S. Richards, Renewable energy-powered membrane technology in Tanzanian communities, Npj Clean Water 1 (1) (2018) 24.
[19] E. Ogunniyi, B.S. Richards, Renewable energy powered membrane technology: Power control management for enhanced photovoltaic-membrane system performance across multiple solar days, Appl. Energy 371 (2024) 123624.
[20] Y.-A. Boussouga, R.L. Ramos, E. Ogunniyi, B.S. Richards, A.I. Schäfer, Energy efficiency of single-pass electrodialysis and nanofiltration/reverse osmosis for brackish water desalination: An experimental comparison, Desalination 621 (2026) 119670.
[21] M. Hoyer, D. Zabelt, R. Steudtner, V. Brendler, R. Haseneder, J.U. Repke, Influence of speciation during membrane treatment of uranium contaminated water, Sep. Purif. Technol. 132 (2014) 413–421.
[22] C.B. Yazzie, C. Elias, V. Karanikola, Uranium rejection with nanofiltration membranes and the influence of environmentally relevant mono- and divalent cations at various pH, Environ. Sci.: Water Res. Technol. 10 (9) (2024) 2075–2086.
[23] H.M.A. Schulte-Herbrüggen, A.J.C. Semião, P. Chaurand, M.C. Graham, Effect of pH and pressure on uranium removal from drinking water using NF/RO membranes, Environ. Sci. Technol. 50 (11) (2016) 5817–5824.
[24] H.M.A. Rossiter, M.C. Graham, A.I. Schäfer, Impact of speciation on behaviour of uranium in a solar powered membrane system for treatment of brackish groundwater, Sep. Purif. Technol. 71 (1) (2010) 89–96.
[25] M.G. Torkabad, A.R. Keshtkar, S. Safdari, Comparison of polyethersulfone and polyamide nanofiltration membranes for uranium removal from aqueous solution, Prog. Nucl. Energy 94 (2017) 93–100.
[26] G. Forchhammer, IV. On the Composition of Sea-water in the Different Parts of the Ocean vol. 155, Philosophical Transactions of the Royal Society of London, 1865, pp. 203–262.
[27] S. Banerjee, B. Mordina, P. Sinha, K.K. Kar, Recent advancement of supercapacitors: a current era of supercapacitor devices through the development of electrical double layer, pseudo and their hybrid supercapacitor electrodes, J. Energy Storage 108 (2025) 115075.
[28] J. Zhang, M. Gu, X. Chen, Supercapacitors for renewable energy applications: a review, Micro and Nano Engineering 21 (2023) 100229.
[29] W. Yuan, X. Chen, Z. Yu, Y. Wan, J. Lin, W. Ye, Critical review of membrane fouling in reverse osmosis treatment: Characterizations, models, mechanisms, and controls, Sep. Purif. Technol. 363 (Part 2) (14 August 2025) 132119.
[30] DuPont, FILMTEC Reverse Osmosis Membranes: Technical Manual, 2025 https://www.dupont.com/content/dam/water/amer/us/en/water/public/documents/en/RO-NF-FilmTec-Manual-45-D01504-en.pdf (accessed 24/11/2025).
[31] Nitto Hydranautics, HYDRACoRe10 and 50 LD 4040 Series, 2018 https://membranes.com/wp-content/uploads/Documents/Element-Specification-Sheets/NF/HYDRACoRe/HYDRACoRe10-and-50-LD-4040-Series.pdf (accessed 24/11/2025).
[32] L. Wang, T. Cao, J.E. Dykstra, S. Porada, P. Biesheuvel, M. Elimelech, Salt and water transport in reverse osmosis membranes: beyond the solution-diffusion model, Environ. Sci. Technol. 55 (24) (2021) 16665–16675.
[33] V.G. Gude, Energy consumption and recovery in reverse osmosis, Desalin. Water Treat. 36 (1–3) (2011) 239–260.
[34] B.S. Richards, G.L. Park, T. Pietzsch, A.I. Schäfer, Renewable energy powered membrane technology: Safe operating window of a brackish water desalination system, J. Membr. Sci. 468 (2014) 400–409.
[35] P. Feron, The use of windpower in autonomous reverse osmosis seawater desalination, Wind Eng. (1985) 180–199.
[36] S. Li, A. Voigt, A.I. Schäfer, B.S. Richards, Renewable energy powered membrane technology: energy buffering control system for improved resilience to periodic fluctuations of solar irradiance, Renew. Energy 149 (2020) 877–889.
[37] J. Barry, N. Munzke, J. Thomas, Power fluctuations in solar-storage clusters: spatial correlation and battery response times, Energy Procedia 135 (2017) 379–390.
[38] H. Steen, Geschichte des modernen Bergbaus im Schwarzwald: Eine detaillierte Zusammenstellung der Bergbauaktivitäten von 1890 bis zum Jahr 2000, BoD–Books on Demand GmbH, Norderstedt, 2004.
[39] World Health Organization (WHO), Guidelines for Drinking-water Quality: Fourth Edition Incorporating First Addendum, 2017 https://iris.who.int/server/api/core/bitstreams/1b7a285e-3635-45dd-a1a9-6068c8fbe173/content (accessed (accessed on 24/11/2025)).
[40] Bundesministerium der Justiz und für Verbraucherschutz, Verordnung zum Schutz vor der schädlichen Wirkung ionisierender Strahlung (Strahlenschutzverordnung - StrlSchV), 2018 https://www.gesetze-im-internet.de/strlschv_2018/StrlSchV.pdf.
[41] E.E. Chang, C.-H. Liang, C.-P. Huang, P.-C. Chiang, A simplified method for elucidating the effect of size exclusion on nanofiltration membranes, Sep. Purif. Technol. 85 (2012) 1–7.
[42] T.R. Nickerson, E.N. Antonio, D.P. McNally, M.F. Toney, C. Ban, A.P. Straub, Unlocking the potential of polymeric desalination membranes by understanding molecular-level interactions and transport mechanisms, Chem. Sci. 14 (4) (2023) 751–770.
[43] J.O. Ighalo, Z. Chen, C.R. Ohoro, M. Oniye, C.A. Igwegbe, I. Elimhingbovo, B. Khongthaw, K. Dulta, P.-S. Yap, I. Anastopoulos, A review of remediation technologies for uranium-contaminated water, Chemosphere 352 (2024) 141322.
[44] C. Xing, B. Bernicot, G. Arrachart, S. Pellet-Rostaing, Application of ultra/nano filtration membrane in uranium rejection from fresh and salt waters, Sep. Purif. Technol. 314 (2023) 123543.
[45] M. Verma, V.A. Loganathan, Insights on the mechanism of uranium removal via nanofiltration in alkalinity and salinity dominated groundwater systems, Water Air Soil Pollut. 235 (4) (2024) 256.